Wetting Dynamics in Multiscale Porous Media. Porous Pore-Doublet Model, Experiment and Theory

T. Staffan Lundström and L. Håkan Gustavsson
Division of Fluid Mechanics, Dept. of Mechanical Engineering, Luleå University of Technology, SE-971 87 Luleå, Sweden

Normunds Jēkabsons and Andris Jakovics
Laboratory for Mathematical Modeling of Environmental and Technological Processes, Dept. of Physics and Mathematics, Latvia University, LV-1002,8 Zellu str., Riga, Latvia

DOI 10.1002/aic.11387
Published online December 26, 2007 in Wiley InterScience (www.interscience.wiley.com).

Fiber reinforced composite materials often consist of fibers gathered in bundles. Thus, during manufacturing, a liquid resin impregnates a multiscale porous medium. For wetting systems the capillary pressure jump becomes much higher in the smaller pores, i.e., within the bundles, and in addition to any applied pressure gradient there will be a local driving pressure gradient between the small- and large-scale areas. Such gradients will influence mechanisms, such as void formation and particle filtration. Hence, it is of interest to clarify the mechanisms for the wetting in general and the influence from the detailed geometry of the fiber network in particular. In this article, a porous pore-doublet model is studied in order to determine if an overflow of liquid can explain a leading flow in the smaller capillaries, and at which conditions it takes place. Experiments, as well as theoretical calculations on this generic geometry show that the leading front can be in the smaller capillary, as well as in the larger one. The outcome is dependent on the actual permeability of the porous material being a parameter that determines to what extent the larger capillary feeds the smaller one.
 AIChE J, 54: 372–380, 2008
Keywords: wetting, wicking, capillary, void formation, multiscale, pore-doublet

Introduction

It is well established that voids are formed at liquid flow fronts when resins impregnate fiber reinforcements.[1–4] The reason for this is that the fibers are clustered in bundles, and the resin will move faster in some areas eventually enclosing gas in other areas.[1,2] It has been shown that when capillary actions dominate the impregnation, the leading flow front is in the smaller capillaries within the bundles, while when an applied pressure takes over, the larger capillaries formed between the bundles are filled first.[4] This interesting behavior can be studied by usage of the pore-doublet model.[5] The model consists of one capillary being branched off into a small, and a large one that after a certain distance rejoin; cf. Figure 1. The model was derived already in 1956,[5] but has recently been extended to deal with inertia effects appearing at large Reynolds numbers.[6] It is obvious that as long as the Reynolds number is low enough, and the driving pressure (capillary or applied) and any body forces are working in the same direction, the liquid will always move faster in the larger capillary. The result of this is that air is entrapped in the smaller capillary. Hence, the original form and the

Correspondence concerning this article should be addressed to S. Lundström at staffan.lundstrom@ltu.se.

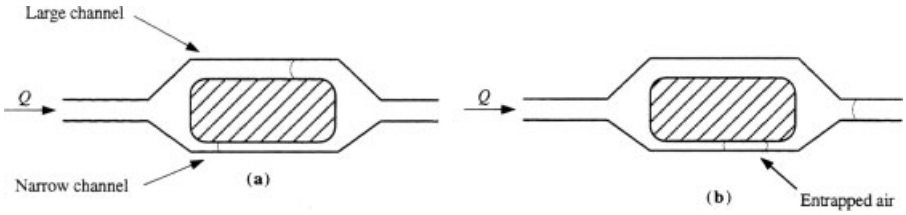

Figure 1. Pore-doublet model when a wetting liquid displaces air.

extended version of the pore-doublet model can, consequently, not explain the observations made in.[4]

A main difference between the pore-doublet model in its original form and various-sized capillaries in real fiber reinforcement, is that the latter are connected, often continuously. Hence, a large capillary can feed a smaller one. It will here be investigated if such an overflow of liquid can explain a leading flow in smaller capillaries, and at which conditions this takes place. Focus is set on the pore-doublet model in its original form, but with a porous channel between the capillaries, hence, a porous pore-doublet model, the pp-doublet model.

Experimental

To mimic the geometry of the pore-doublet model two notches were formed in a PMMA plate. The depths of the notches is about 1 and 2 mm, respectively, and they are positioned in parallel 6 mm apart (see Figure 2). This setup made it possible to put a porous material between the notches through which the experimental liquid could flow from one capillary to the other. Two types of porous material were used. The first was a metal net positioned between the capillaries. The net consisted of metal wires having a diameter of about 60 μm in a plain weave. The second porous material was obtained by scratching very shallow cross-flow channels between the capillaries. By this technique the capillaries are still connected by a sort of porous medium without a driving capillary pressure in the main flow direction. In all experiments the porous material and the capillaries were sealed with a tape (see Figure 2). As experimental liquid 95% Ethanol was used due to its very good wetting behavior ($\mu = 4\ \mu Pa \times s$ and $\gamma_{lv} = 22.8\ mN \times m^{-1}$ at 20°C; tabulated values for 99% Ethanol). The plate was put horizontally on a table to minimize the effect from gravity and the capillaries were attached to an unlimited liquid supply. The supply was leveled with the capillaries so that the fluid moved by capillary action only. To secure the registration of the relatively fast movement of the liquid through the capillaries all experiments were videotaped with a Panasonic F15 HS video camera connected to a video recording system.

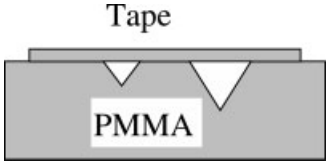

Figure 2. Cross-section of PMMA-plate with capillaries.

We will here present the outcome of three sets of experiments. In the first experiment the liquid was allowed to flow into the capillaries and weave separately. As derived from the Washburn Eq. 7, the liquid then moves slower in the smaller capillary as compared to the larger one. This is evident from Figure 3 where it is also observed that the front moves even slower in the weave. The reason for this is that the resistance to flow in smaller capillaries dominates over the higher capillary pressure jump at the flow front. Furthermore, the plots of the fronts in the larger and smaller capillary have a perfect fit to a straight line (the regression is 0.999 and 0.998 in respective capillary). This indicates that the notches have a uniform cross-section in the flow direction.

In the second experimental setup the weave was put between the capillaries, making it possible for the liquid to move between the capillaries through the weave. As apparent from Figure 4 the situation is now completely different; the flow in the weave is leading with a speed about four times that obtained when it is not connected to the capillaries. Also, at the last two measuring points all fronts in this experiment move faster than the front in the smaller capillary in the previous experiment. Hence, there is a developed flow between the capillaries.

In the third experimental setup the weave was removed and the capillaries were connected through the cross-flow channels previously described. When the density of these notches is fairly low (one every 5 mm), giving a low-permeability, the liquid moves fastest in the larger capillary (cf. Figure 5). When increasing the permeability by doubling the number of notches, it is from the beginning no longer possible to distinguish which front is leading. Eventually the front

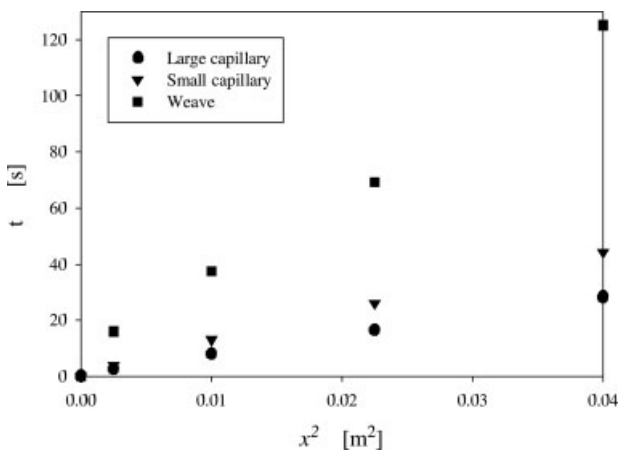

Figure 3. Fluid front position when the capillaries are separated: the temperature was 22.3°C.

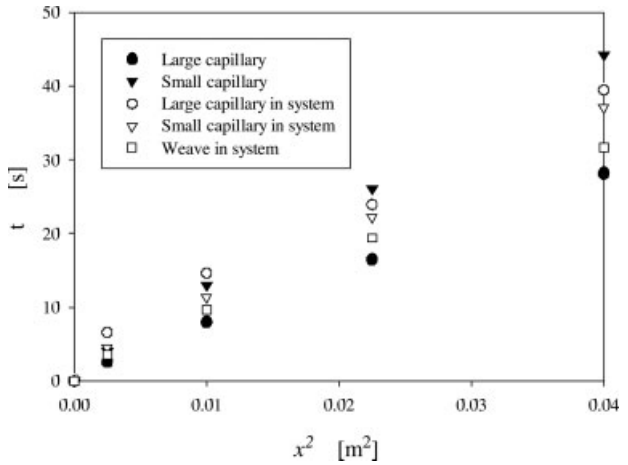

Figure 4. Fluid front position when the capillaries are connected with the weave: the black symbols denote results from Figure 3; the temperature was 22.3°C.

in the smaller capillary takes the lead. Hence, it is obvious that the location of the leading front is dependent on the resistance to flow in the material between the capillaries.

The experiments were repeated to confirm the results, but are still associated with some uncertainties. The major errors are temperature variations and differences in the level of liquid in the supplying beaker. However, neither of these variations influence the comparisons presented. The temperature was, for instance, the same for the first two experimental setups, 22.3 °C, while it increased somewhat during the third, 24.2 °C. This might be one reason why the liquid moves faster in the larger capillary in the third series as compared to the first experiment (cf. Figure 3 and Figure 5). The maximum variation in the level of the liquid supply is estimated to 0.5 mm. This will result in a driving pressure of less than 5 Pa, as compared to the pressure jump at the larger capillary front approximated to be around 50 Pa. Hence, the maximum error in the driving pressure is roughly 10%, and, thus, much lower than the differences highlighted in this article.

Theoretical Background

Theoretical models will be derived that can explain some of the observed results. The general assumptions introduced are that:

- The fluid can be treated as Newtonian.
- The Reynolds number is so small that inertia effects can be neglected.
- There is a fully developed Poiseuille flow in the capillaries.
- The scratches are ideally spaced and has uniform cross-section, and the plain weave is homogeneous in its structure.
- The capillary pressure can be described with the following equation

$$\Delta p = -\frac{2\gamma}{r}\cos\theta \tag{1}$$

where neither contact angle θ, nor surface tension modulus γ depend on the local capillary surface velocity v.

- Darcy's law is applicable for flow in the weave.

Following the third assumption above the flow rate in the capillaries can be derived from the following expression

$$Q = -\alpha r^4 \frac{dp}{dl} \tag{2}$$

where p denotes pressure, and l is the length along the capillary with characteristic sectional size r. In the case of a circular cross-sectional area, r can be chosen as the radius of the capillary, and $\alpha = \pi/8\mu$. The average velocity in such a tubular capillary, is, thus, given by

$$\bar{v} = \frac{Q}{\pi r^2} = -\frac{\alpha r^2}{\pi}\frac{dp}{dl}. \tag{3}$$

Let R_1 and R_2 denote the radii for the respective capillary, and p_1, p_2 represent the corresponding pressures. Then the flow rates within each capillary become

$$Q_1 = -\alpha R_1^4 \frac{dp_1}{dx}; \quad Q_2 = -\alpha R_2^4 \frac{dp_2}{dx}. \tag{4}$$

These rates depend on the flow from the capillaries to the weave, and will be denoted as q_i, $i = 1, 2$: where q_1 and q_2 correspond to capillary 1 and 2, respectively. Continuity now yields that these flow rates can be expressed as

$$\frac{dQ_1}{dx} = -q_1, \quad \frac{dQ_2}{dx} = -q_2 \tag{5}$$

which combined with Eq. 4 yields

$$\alpha R_1^4 \frac{d^2 p_1}{dx^2} = -q_1, \quad \alpha R_2^4 \frac{d^2 p_2}{dx^2} = -q_2. \tag{6}$$

The flow rates from the capillaries to the porous medium q_1, q_2 depend on the internal geometry. In the case of a weave, Darcy's law may be written as

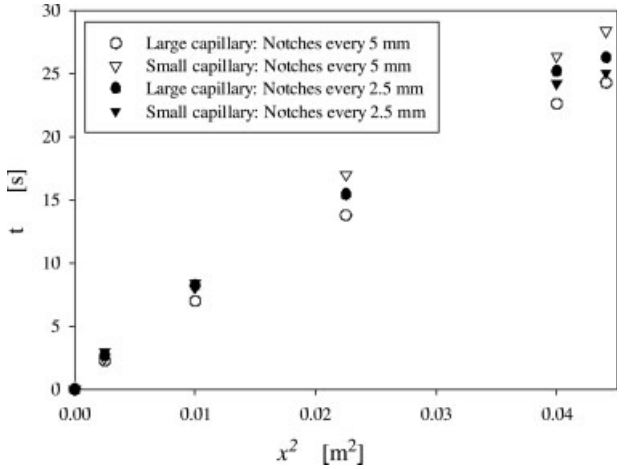

Figure 5. Fluid front position when the capillaries are connected with tiny notches every 5 mm (open symbols) and 2.5 mm (filled symbols): the temperature was 24.2°C.

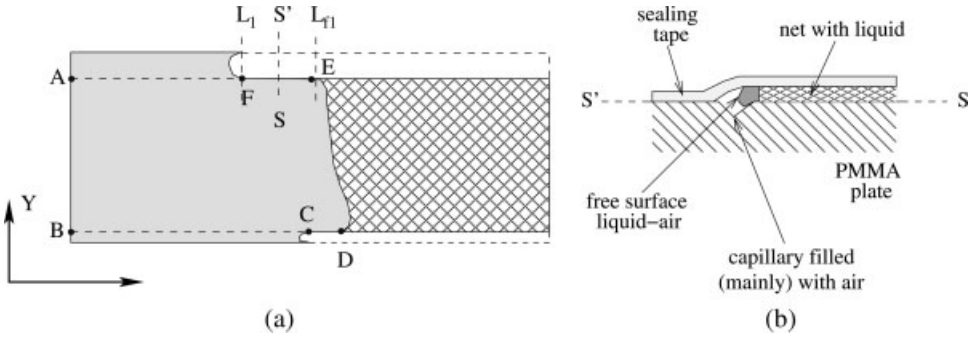

Figure 6. (a) Capillaries connected with weave: The contour ABCDEF encloses porous media (net), which is filled with liquid; (b) capillaries connected with weave: the concept of free microsurface in the section SS' between capillaries and the net.

$$q = -\frac{k}{\mu}\text{grad}_n p \tag{7}$$

where $\text{grad}_n p$ is the pressure gradient component in the weave, normal to the boundary, and k is the permeability of the weave. The homogenized velocity in the weave is related to q via the porosity Π

$$v = q/\Pi. \tag{8}$$

For the scratched notches the situation is similar. If the notches have circular cross-section the flow rate in respective capillary may be expressed as

$$q_i = -r_n^4 \frac{\alpha}{\Delta l_n}\frac{dp_i}{dy} \quad \forall i : i = 1, 2 \tag{9}$$

where r_n is the average radius of the notch, and $1/\Delta l_n$ is the spatial frequency between two neighbor notches (notch density). The derivative in Eq. 9 is taken along the notch.

The case with notches and the flow between the capillaries will be dealt with in the Modeling of the Flow in the Capillaries section. It will, however, first be shown how the theoretical concepts introduced above can explain why the flow front always leads in the net.

Modeling of the Flow in the Weave

Consider, the dimensionless form of Darcy's law in the weave according to

$$\mathbf{v}^* = -\text{grad}\, p^* \tag{10}$$

where the pressure p^* is normalized so that $p^* = 1$ on the moving weave/air boundary. From Eq. 10, and mass conservation of an incompressible liquid, the 2-D Laplace equation can be formed in the following way

$$\frac{\partial^2 p^*}{\partial x^2} + \frac{\partial^2 p^*}{\partial y^2} = 0 \tag{11}$$

which applies to the pseudo-2-D domain of the weave as shown in Figure 6a.

The boundary conditions are crucial for the model. At the inlet, on the segment AB atmospheric pressure is applied implying $p_0^* = 0$. On the boundaries shared with each channel, BC and FA, Eqs. 6, 7 and 8 are valid, leading in general to boundary conditions of mixed type. To demonstrate the concept it is assumed for simplicity that the capillaries have much higher liquid transport capabilities as compared to the weave, a situation common in composites manufacturing. Notice that the draining effect itself will be analyzed in the next chapter. With the assumption earlier presented, zero inlet pressure and Eq. 1 as boundary condition on the free capillary surfaces, Eq. 6 has a simple linear solution according to

$$p_i^* = -\frac{x}{L_i^* R_i^*} \tag{12}$$

where the dimensionless radii R_i^* are normalized, with $R_i^* = R_i/r_{pore\ eff}$ and L_i^* are the positions of the free surfaces in the capillaries, the points C ($x = L_1^*$) and F ($x = L_2^*$). Thus, Eq. 12 serves as boundary conditions on segments BC and FA in the model, while the boundary condition on the free surface DE corresponds to the initial normalization $p^*|_{DE} = 1$. The conditions on CD and EF have to ensure L^0 continuity of p^* along the closed contour Γ_1 = ABCDEF. Thus, although p^* must have a unique value everywhere, infinite tangential derivative of p^* can be allowed at isolated points of Γ_1. It can be proven that the statement previously ensures a finite mass transport on any segment of Γ_1. The L^0 continuity of p^* is valid on the contour points A and B where there is no interphase boundary. Similarly, points D and E lie on the boundary between the net and air, and, thus, the same capillary pressure exist in both contour directions. However, at points C and F capillaries with large radii are bound together with the much finer net, the weave. A simple formal approach by substituting the characteristic size in a $1/r$ pressure multiplier of the capillary pressure formula Eq. 1, leads to pressure jumps at points C and F, and corresponding nonphysical infinite local velocities. Let us instead, in a physically reasonable way, assume that the free surface of liquid inside an internal volume can take up a shape, which eliminates unrealistic velocities, and let us describe that shape in the simplest way possible. For geometric reasons it is likely that the net curvature radii change significantly when the liquid approaches the edge of the capillary (see Figure 6b). Hence, the

capillary pressure on these boundary lines can dramatically change with a small liquid consumption. Thus, the following statement is introduced

$$\left.\frac{\partial p^*}{\partial \mathrm{n}}\right|_{CD,EF} = 0 \tag{13}$$

In fact Eq. 13 always ensures a leading position of the liquid front in the weave near the edges, thus, $L^*_{fi} > L^*_i$ where $x = L^*_{f1}$ on D, and $x = L^*_{f2}$ on E, Figure 6a. However, in the middle of DE the free surface may lag. Thus, depending on the shape an average position of the liquid front DE in the weave can lead or lag with respect to the fronts in the capillaries.

In order to determine the exact shape of the free boundary DE numeric simulations are performed by applying the boundary element method (BEM) to Eq. 11. This method implies a division of the domain boundary into segments of finite length—boundary elements. For each j-th element some fictive "charge density" (the term is borrowed from BEM solution of electrostatic problem; for a more detailed discussion and BEM theory see Refs. 8 and 9) $\rho_j(x_j,y_j)$ is chosen with respect to the applied boundary conditions. In order to obtain smooth derivatives on the boundary contour these "charges" are set on an outer contour Γ_2, which surrounds Γ_1 lying near to it. Since Γ_2 closely resembles Γ_1 it is not shown in the figure. Finally, the pressure in each point inside the contour Γ_1 is expressed as

$$p^*(x,y) = \sum_j G_j(x - x_j, y - y_j)\rho^*_j \tag{14}$$

where $G_j(x,y)$ is an analytical solution of a potential of a uniformly charged infinite plate being oriented in the XY plane in the same way as a corresponding j-th. boundary segment of Γ_2. The values of ρ^*_j are obtained from boundary conditions Eqs. 12 and 13 by solution of the linear system: $A_{ij}\rho_j = B_j$ with a fully populated matrix A for each time step.

Also at each time step the free boundary DE is moved by $\mathbf{v}\Delta t$, where the local velocities $\mathbf{v}$ on DE of Γ_1 are given by Eq. 10. Only the x-coordinate of the moving boundary point is affected via special polynomial mapping algorithms allowing $\{v^*_x, v^*_y\} \rightarrow \{v^*_x,0\}$ on the free boundaries. Notice that capillary meniscus positions (points C and F in Figure 6a) may be expressed as

$$(L^*_i)^2 = 2cR^*_i t + (L^*_{i0})^2, \quad i = 1,2 \tag{15}$$

where L^*_{i0} is the initial values of L^*_i, and c is a constant of unit order of magnitude. Here c is set to unity, and $R^*_1 = R^*_2 = 4$. The spacing between the capillaries are normalized independently, $|\mathrm{AB}| = 1$ together with time scale selection, to ensure Eq. 10.

The square of the predicted fluid front average position in the weave has an almost linear relationship with time (see Figure 7), and the distance between the free surfaces in, respectively, capillary, and the weave increases with time in conformity with experimental data (cf. Figure 4). In addition, the capillary flow front positions C and F are between those for the weave in the system and the unconnected weave, confirming the experimental results in Figures 3 and 4.

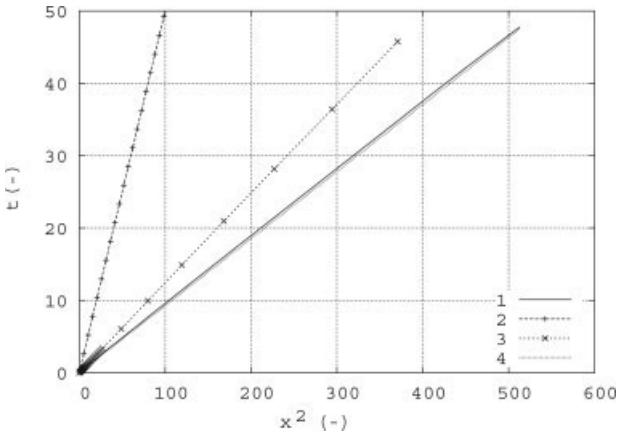

Figure 7. Square of modeled dimensionless fluid front position in the weave as a function of dimensionless time when the capillaries are of equally size: (1) averaged front position in the weave in the system; (2) averaged front position in the weave with no supply of liquid from the capillaries; (3) position of capillary fronts, points C and F; and (4) analytically computed front position in the weave using Eqs. 17 and 18.

Due to the assumptions $L^*_1 = L^*_2$, $L_{1f} = L_{2f}$ and $p^*_1 = p^*_2$ the velocity of the corner points $v_c = dL^*_{f1}/dt = dL^*_{f2}/dt$ can be roughly approximated with

$$\frac{dL^*_{fi}}{dt} = \frac{1 - p^*_i}{L^*_{fi} - L^*_i}, \quad i = 1,2 \tag{16}$$

which with substitution of Eqs. 12 and 15 for L^*_{fi} yields the following self-consistent albeit partial solution

$$\left(L^*_{f1}\right)^2 = \left(L^*_{f2}\right)^2 = 2\kappa^2 t + \kappa^2\left(L^*_{01}\right)^2/R^*_1 \tag{17}$$

where κ is a solution of

$$\kappa^2 - \kappa\sqrt{R^*_i} + 1/R^*_1 = 1 \tag{18}$$

The solution of Eqs. 17 and 18 is shown in Figure 7 as a curve labeled "analytic". The agreement is rather good on late front development stages ($x^2 > 1$, $t > 1$), on which the aforementioned expressions can be used for the estimation of weave leading effects. In earlier stages the fluid front in the weave is far from being a straight line (see Figure 8), where BEM predicted front shapes at some averaged front positions are shown. Notice the retardation of the front in the middle of the region, when liquid feeding from capillaries is low. Thus, for small t, x Eqs. 17 and 18 are evidently invalid. However, for large x the shape of the front is almost a straight line (with a linear p distribution between L^*_1 and L^*_{if}), in agreement with the famous St. Venant mechanics principle. In such a case Eqs. 17 and 18 can be used as analytic criterion for leading flow positions in the weave. For more general cases (for example, with a nonzero injection pressure

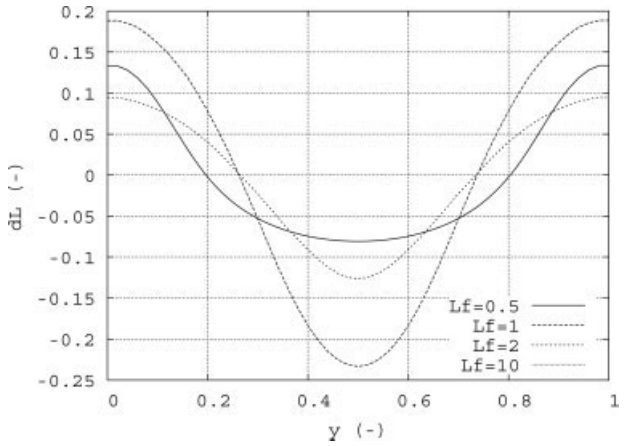

Figure 8. BE model predicted shape of free boundary in the, weave regarding the model case with equally sized capillaries.

On the horizontal axis—width of the weave, on the vertical axis—front deviation from its average position. The shapes correspond to average corner point positions, Lf, of 0.5, 1, 2 and 10 units.

p_0^*, and nonisotropic permeability of the weave), it is of course possible to solve Eq. 16 in an iterative way.

Modeling of the Flow in the Capillaries

The model presented in the previous section cannot explain that the flow front in one capillary overtakes the lead from the other capillary. In order to develop such a model, finite q_i are introduced for the pp-doublet problem when the porous medium consists of scratched notches (see Figure 9). This case is chosen for analysis principally because of its simplicity allowing for direct analytical approaches.

Two mathematical models are developed. The first one is semianalytic, and can be used for parametric studies. Here, rather rough assumptions are utilized in order to have a result in the form of closed expressions. In the second model, numeric methods are used so that liquid front positions can be predicted in a more accurate way, thus, validation of the main concepts can be achieved.

Analytic model

In the domain $x < L_0$ all notches are completely filled with the fluid, therefore,

$$\frac{dp_1}{dy} = -\frac{dp_2}{dy} = \frac{p_2 - p_1}{l*} \tag{19}$$

where l^* is the distance between the capillaries. Then Eq. 6 together with Eqs. 9 and 19, yield the following system of second-order linear differential equations

$$\frac{d^2p_1}{dx^2} = \beta_1(p_1 - p_2) \tag{20}$$

$$\frac{d^2p_2}{dx^2} = \beta_2(p_2 - p_1) \tag{21}$$

where the constants β_1 and β_2: $\beta_i = r_n^4\ (R_i^4 l^*\ \Delta l_n)^{-1}$ are only dependent on geometric characteristics of the capillaries and the porous medium, the notches.

The general solution of Eq. 21 is

$$p_i = (-1)^i \beta_i [K_1 \sinh(\lambda x) + K_2 \cosh(\lambda x)] + K_3 x + K_4, \quad \forall i : i = 1, 2 \tag{22}$$

in which $\lambda = \sqrt{\beta_1 + \beta_2}$, and where the constants K_1, K_2, K_3 and K_4 are determined by applied boundary conditions. For simplicity, the pressure scale is shifted so that the atmospheric pressure vanishes

$$p_1|_{x=0} = p_2|_{x=0} = 0. \tag{23}$$

These relationships can be satisfied by Eq. 22 if $K_2 = K_4 = 0$.

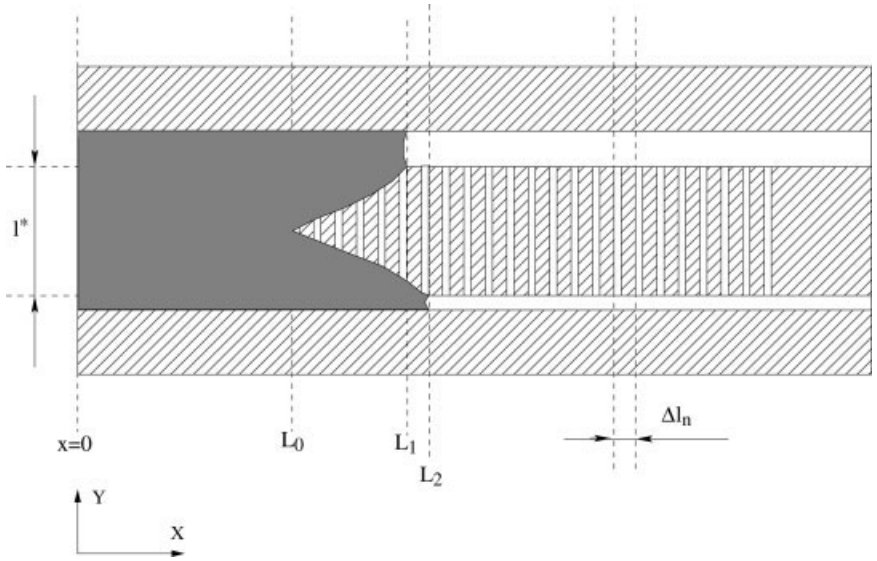

Figure 9. Possible advance scenario of fluid front in the system of scratched notches.

The length L_0 defined in Figure 9 is naturally the same for both capillaries, while the boundary conditions on $x = L_0$ differ according to

$$p_1|_{x=L_0} = p_1^{L_0}; \quad p_2|_{x=L_0} = p_2^{L_0} \tag{24}$$

leading to the following expressions for K_1 and K_3

$$\begin{aligned} K_1 &= \frac{1}{\lambda^2}\frac{p_2^{L_0} - p_1^{L_0}}{\sinh(\lambda L_0)} \\ K_3 &= \frac{1}{\lambda^2}\frac{p_2^{L_0}\beta_1 + p_1^{L_0}\beta_2}{L_0} \end{aligned} \tag{25}$$

The average velocity in respective capillary can be obtained by differentiation of Eq. 22. From Eqs. 3, 22 and 25 it follows that

$$\bar{v}_i = -\frac{\alpha R_i^2}{\pi\lambda}\left[(-1)^i\beta_i\frac{p_2^{L_0} - p_1^{L_0}}{\sinh(\lambda L_0)}\cosh(\lambda x) + \frac{p_2^{L_0}\beta_1 + p_1^{L_0}\beta_2}{L_0\lambda}\right], \quad i = 1,2 \tag{26}$$

and, consequently, Eqs. 22 or 26 can be used as a part of a general model in which processes in the region $L_0 < x < L_i$ are described (see Figure 9). However, it is also possible to employ the analytical model alone in order to have some qualitative results. Then it needs to be assumed that the following inequalities hold

$$\left|\int_{L_0}^{L_i} q_i dx\right| \ll |Q_i(L_i)| \quad \text{and} \quad \frac{p_i(L_i) - p_i(L_0)}{p_i(L_0)} \ll 1 \quad \forall i : i = 1,2 \tag{27}$$

where L_i are positions of the fluid fronts in the respective capillary as shown in Figure 9. The earlier assumptions ensure that the pressures $p_i^{L_0}$ in Eq. 26 are approximately the same as the pressure on the front of the free boundaries, $p_i^{L_i}$ as prescribed by capillary forces Eq. 1

$$p_i^{L_i} = -\frac{2\gamma}{R_i}\cos\theta \quad \forall i : i = 1,2 \tag{28}$$

for respective, i-th capillary. For simplicity, and further on cosθ is set to 0.5. Application of the explicit expression for β_i, and Eqs. 26 to 28 yields the following expression for the velocity at $x = L_0$

$$\bar{v}_i(L_0) = \frac{\kappa r_n^4 R_i^2}{\lambda R_1 R_2}\left[(-1)^i\frac{R_1 - R_2}{R_i^4}\tanh^{-1}(\lambda L_0) + \frac{R_1^3 + R_2^3}{\lambda L_0 R_1^3 R_2^3}\right], \quad i = 1,2 \tag{29}$$

in which κ is independent of geometric quantities, such as R_i and L_j. In the framework of conditions Eq. 27, velocities from Eq. 29 coincide with the speed of the corresponding capillary fronts. The ratio $P = \bar{v}_1(L_1)/\bar{v}_2(L_2)$ can now be expressed as

$$P(\xi,\eta) = \frac{\bar{v}_1(L_1)}{\bar{v}_2(L_2)} = \eta\frac{(1-\eta)\tanh^{-1}(\xi) + (\eta^4 + \eta)\xi^{-1}}{(\eta^4 - \eta^3)\tanh^{-1}(\xi) + (\eta^3 + 1)\xi^{-1}} \tag{30}$$

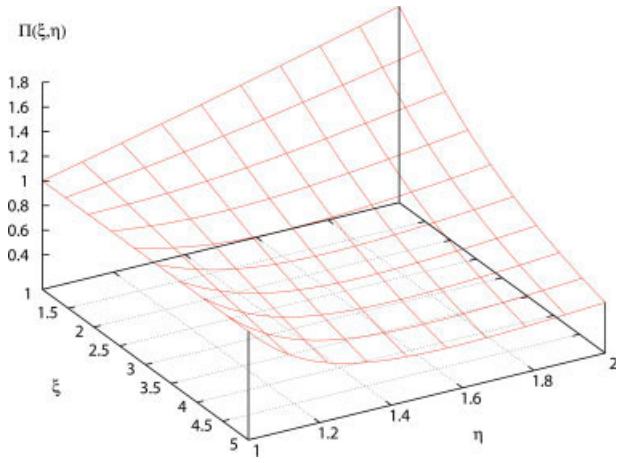

Figure 10. Plot of capillary tubes velocity ratio, P = v1/v2 as function of capillary radii η = R1/R2 and nondimensional average front advance position, ξ, see Eq. 31.

Depending on position in the (ξ, η) plane the fluid front in the smaller capillary advances faster or slower, as compared to the one in the larger capillary. [Color figure can be viewed in the online issue, which is available at www.interscience.wiley.com.]

where the nondimensional quantities ξ, η are defined as

$$\xi = L_0\lambda = L_0\frac{r_n^2}{\sqrt{l^*\Delta l_n}}\sqrt{\frac{1}{R_1^4} + \frac{1}{R_2^4}}; \quad \eta = R_1/R_2 > 1 \tag{31}$$

Now let $1 \le \xi \le 5$, $1 \le \eta \le 2$, and let us study the response of $P(\xi, \eta)$, Eq. 30, see Figure 10. The lower left edge of the P plot lies at a unit distance from the (ξ, η) plane since it corresponds to the case when the radii are equal. The $P(\xi, \eta)$ surface near the top right corner ($\xi = 1$, $\eta = 2$) is located higher than the unity mark of the vertical axis, implying that the flow front in the larger capillary advances faster. To the contrary the region of functional plot of P near the right bottom edge ($\xi = 5$, $\eta = 2$) is below the unit label, indicating that the capillary front in the smaller capillary is leading.

The obtained results, qualitatively agree with experimental observations since L_0 Eq. 31 increases with ξ values, and for low L_0, the front in the larger capillary is expected to be faster. While for high L_0, the front in the smaller capillary should lead (cf Figure 5).

Such a tendency is readily understood. The number of filled scratches, and, therefore, connections between the capillaries increase with L_0. For small values of L_0 the capillaries have a weak connection, and can be treated as separate objects. The capillary pressure is proportional to the radius of capillary, $1/R$, while the hydrodynamic resistance is proportional to R^{-2}, therefore, the capillary front speed is proportional to R: $\bar{v}(x = L_0) \propto R^{-1}/R^{-2} = R$, i.e., the larger capillary is supposed to have faster liquid speed. Now consider that both capillaries are well connected through the notches as is the case of large L_0. The fluid tank is far from the capillary surfaces, and the smaller capillary may drain the larger one through the notches due to higher capillary

Table 1. Model Parameters

	r_n (mm)	R_1 (mm)	R_2 (mm)	l^* (mm)	Δl_n (mm)	$\alpha \times 10^{-4}$ $1/(Pa \cdot s)$	γ mPa/m
Fig. 11	0.3	1	2	6	5	5.44	22.8
Fig. 12	0.3	1	2	6	2.5	5.44	22.8

pressure. Now the larger capillary may take a role of a major fluid contributor, feeding the advancement of both capillary fronts. In competition for the common fluid supply the larger capillary has lower driving force, and, likewise, a slower capillary front.

Another interesting feature of the simplified model, and particularly of Eq. 30, are negative $P(\xi, \eta)$ values in the case of large ξ, which corresponds to negative flow in one of the capillaries. The condition for $P(\xi, \eta) < 0$ is

$$\frac{\xi}{\tanh(\xi)} \geq \frac{\eta^4 + \eta}{\eta - 1} \tag{32}$$

Condition Eq. 32 corresponds to a very distant liquid supply, thus, it is stated that at the point of equality of Eq. 32, the fluid front in larger capillary will stop.

Finite difference model

The model described previously is constrained by assumptions Eq. 27. For more exact front position predictions in the pp-doublet model studied, a finite difference (FD) method based numeric model is developed.

The grid used has the same period as the mesh of scratched notches. Each notch may be empty, partially filled or fully filled with liquid. By definition a fully filled n-th notch has position $x_n = n\Delta l_0 < L_0$ (see Figure 9). The finite difference equivalent of Eq. 21 may now be formed as

$$\left(p_{i,n+1} - p_{i,n}\right)/\Delta^+ + \left(p_{i,n-1} - p_{i,n}\right)/\Delta^- = \Delta^{\pm}\beta_i\left(p_{i,n} - p_{j,n}\right) \tag{33}$$

where all three spatial differences Δ^+, Δ^- and $\Delta^{\pm} = (\Delta^+ + \Delta^-)/2$ are equal to Δl_n since the mesh of notches is equally spaced, $i \neq j$, $i, j = \{1,2\}$, and n is the number of the notch.

In the domain of partially filled notches, $L_0 \leq x \leq \max(L_1, L_2)$, Eq. 21 has to be replaced by

$$\frac{d^2 p_i}{dx^2} = \frac{\beta_i l^*}{l_i^n}\left(p_i + \frac{\gamma}{r_n}\right) \tag{34}$$

where l_i^n is the length of the filled part of the n-th notch from the side of the *i-th* capillary.

The finite difference equivalent of Eq. 34 is

$$\left(p_{i,n+1} - p_{i,n}\right)/\Delta^+ + \left(p_{i,n-1} - p_{i,n}\right)/\Delta^- = \Delta^{\pm}\frac{\beta_i l^*}{l_i^n}\left(p_{i,n} - p_n\right) \tag{35}$$

being similar to Eq. 33. However, since the position of the free surfaces L_i may be arbitrary: $L_i > L_0$ the Δ^+ and $\Delta^{\pm}$ are not equal to Δl_n in this case.

Systems 33 and 35 are solved at each time step, and the velocities in each capillary on front positions L_1 and L_2 are obtained from the FD equivalent of Eq. 3. Similarly the average liquid speed in an individual nonfilled notch $L_0 \leq x_n \leq L_i$ is calculated from

$$\bar{v}_n = -\frac{\alpha r_n^2}{\pi} \times \frac{p_n - p_i(x_n)}{l_i^n} \tag{36}$$

Then the following numeric integration gives the positions of the capillary surfaces in, respectively, capillary L_1, L_2

$$L_i(t_{k+1}) = L_i(t_k) + \bar{v}_i(t = t_k, x = L_i)dt \tag{37}$$

and the partially filled notches for the next time-step $t_{k+1} = t_k + dt$. After integration, the amount of liquid within each partially filled notch is checked. If $l_1^n + l_2^n \geq l^*$ then the n-th. capillary is marked as completely filled. Finally L_0 is updated so that it follows the notch that is just to be entirely filled.

The model constants used for the simulation are presented in Table 1, where the geometric characteristics are taken as close as possible to the experiments, and the physical constants α and γ are derived from t,x^2 fittings to the experiment with single capillaries (see Figure 3).

The results from the numerical modeling are shown in Figure 11 and Figure 12. In Figure 11, the distance between the notches are 5 mm, while in Figure 12, this distance is just 2.5 mm. In contrast to the unconnected capillaries the square of the positions are not linearly dependent on time anymore. In the first case, Figure 11, the liquid front in the smaller capillary just approaches the liquid front in the larger capillary. In the second case, Figure 12, capillaries are interconnected to a larger extent, as a result L_1 and L_2 curves have a cross-point as also obtained in the experiments. By further comparisons with the experimental curves plotted in Figure 5, it can be concluded that modeled results are in qualitative agreement with observations, while there are

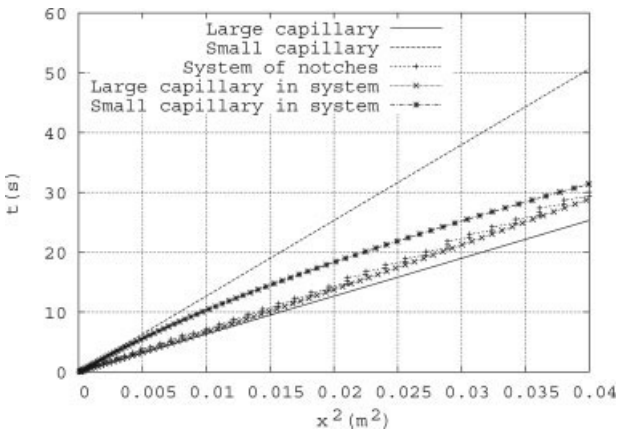

Figure 11. Modeled front advance scenario in pp-doublet problem with scratched notches, notch density 1/5 (notch/mm).

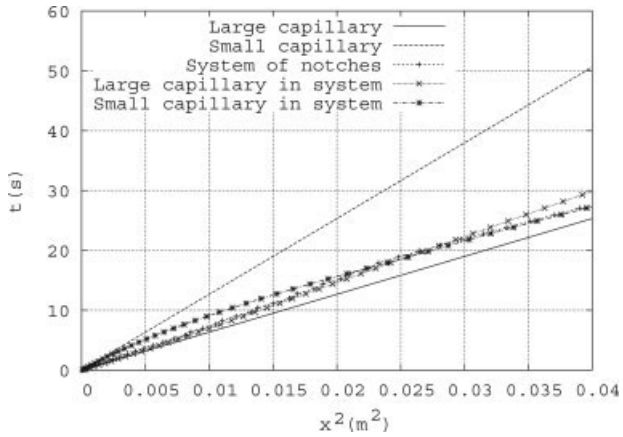

Figure 12. Modeled front advance scenario in pp-doublet problem with scratched notches, notch density 1/2.5 (notch/mm).

some minor quantitative discrepancies. The latter is due to differences in the setups, the capillaries in the model have, for instance, a perfect circular cross-section, while the experimental are more triangular in shape.

In Figure 11 and Figure 12 a L_0 curve is also plotted. A noticeable property of the model used is that this curve is not a smooth function underlining the fact that L_0 jumps from one scratch to another.

Conclusions

Experiments have shown that in a porous pore-doublet model the leading front can be in as well the smaller capillary as the larger one. The outcome is dependent on the actual permeability of the porous material. It may also happen that the front is leading in the porous material. Hence, leading flow-fronts within the denser constituent in a multiscale porous media, such as a fabric used in composites manufacturing, can be explained.

The experimentally observed results are confirmed by relatively simple models that successfully explain the observations presented earlier, thus, it can be stated that the main mechanisms behind porous pore-doublet model in this particular case are known.

Acknowledgments

The experiments were rigorously setup by Allan Holmgren at the Luleå University of Technology. The work was financed by the Swedish Research Council and the Royal Swedish Academy of Sciences.

Notation

α = capillary liquid transport constant
β_1, β_2 = analytic model parameters
Γ_1 = ABCDEF − domain boundary
Γ_2 = fictious domain boundary, used by numeric algorithm of BEM model
γ = surface tension modulus
Δ, Δ^+, Δ^- = forward, backward and centered finite differences
η = dimensionless parameter $\eta = R_1/R_2$
θ = wetting contact angle
κ = geometry independent constant
λ = exponential root of analytic solution
μ = fluid viscosity
ξ = dimensionless parameter
Π = porosity of weave
k = permeability of weave
l = length along capillary
l^* = scratch length
L_0 = position of first completely filled scratch
L_1, L_2, L_i = positions of feeding capillary surfaces
L_1^*, L_2^*, L_i^* = normalized (by weave width) positions of weave feeding capillary surfaces
L_{i0}^* = initial (t=0) dimensionless positions of weave feeding capillary surfaces
L_{f1}^*, L_{f2}^*, L_{fi}^* = dimensionless positions of free boundary at weave corner
$1/\Delta l_n$ = notch scratch frequency
p = local pressure
p^* = normalized pressure
p_1^{L0}, $i = 1,2$ = pressure in capillaries at $l = L_0$
Δp = capillary pressure
Q, Q_1, Q_2 = sectional flow through capillary/capillaries 1,2
q_1, q_2 = capillary (side-)draining flux, m^2/s
R_1, R_2 = radii of feeding capillaries
R_1^*, R_2^* = normalized (by $r_{pore\ eff}$) radii of feeding capillaries
$r_{pore\ eff}$ = effective pore radii, yields experimentally observed free surface speed ratio between unconnected weave and unconnected capillaries
$\underline{v}$ = local velocity
v = average velocity in capillary
v^* = normalized velocity in a net
x, y = coordinates along and transverse main infiltration direction

Literature Cited

1. Parnas RS, Phelan Jr, FR. The effect of heterogeneous porous media on mold filling in RTM. *Sampe Quarterly*. 1991;Jan:53–60.
2. Chan AW, Morgan RJ. A model on formation of rod-like voids in fiber tows. *Sampe Quarterly*. 1993;July:49–53.
3. Lundström TS, Gebart BR. Influence from different process parameters on void formation in RTM. *Polymer Composites*. 1993;15:25–33.
4. Patel N, Lee LJ. Effects of fiber mat architecture on void formation and removal in liquid composite moulding. *Polymer Composites*. 1995;16:386–399.
5. Rose W, Witherspoon PA. Trapping oil in a pore doublet. *Producers Monthly*. 1956;Dec:32–38.
6. Sorbie KS, Wu YZ, McDougall SR. The extended Washburn equation and its application to the oil/water pore doublet problem. *J of Colloid and Interface Sci*. 1995;174:289–301.
7. Washburn EW. The dynamics of capillary flow. *Physical Review*. 1921;17(3):273–283.
8. Jaswon MA, Symm GT. *Integral equation methods in potential theory and electrostatics*. London: Academic Press; 1977.
9. Banerje PK, Butterfield R. *Boundary Element Methods in Engineering Science*. McGraw-Hill Ltd, U.K.; 1981.

Manuscript received Mar. 28, 2007, revision received July 30, 2007, and final revision received Nov. 9, 2007.